

THE ROLE OF ICE COMPOSITIONS AND MORPHOLOGY FOR SNOWLINES AND THE C/N/O RATIOS IN ACTIVE DISKS

ANA-MARIA A. PISO¹, KARIN I. ÖBERG¹, JAMILA PEGUES²

Draft version January 25, 2016

ABSTRACT

The elemental compositions of planets define their chemistry, and could potentially be used as beacons for their formation location if the elemental gas and grain ratios of planet birth environments, i.e. protoplanetary disks, are well understood. In disks, the ratios of volatile elements, such as C/O and N/O, are regulated by the abundance of the main C, N, O carriers, the ice environment in which these carriers reside, and the presence of snowlines of major volatiles at different distances from the central star. We explore the effects of dynamical processes, molecular compositions and abundances, and the ice morphology of dust grains in disks on the snowline locations of the main C, O and N carriers, and their consequences for the C/N/O ratios in gas and dust throughout the disk. We find that radial drift and accretion alone can reduce the snowline radii of the main C, O and N carriers, i.e. H₂O, CO₂, CO and N₂, by 40-60% compared to static disks. If CO and N₂ are bound to water ice instead of pure ices, their snowlines move inward by $\sim 70\%$. Both of these effects substantially change the disk regions where C/O and N/O are enhanced over the stellar value. In the outer disk, the gaseous C/O and N/O are enhanced by factors of ~ 2 and ~ 3 , respectively. Our estimates for the C/N/O ratios are only modestly affected by the presence of some C in the form of CH₄ and of some N in the form of NH₃.

1. INTRODUCTION

1. The chemical composition of protoplanetary disks is largely dictated by the freeze-out of volatile species, such as carbon, oxygen and nitrogen carriers.
2. Carbon and oxygen bearing molecules, such as H₂O, CO₂ and CO, as well as the C/O ratio in protoplanetary disks/giant planet atmospheres have been extensively studied from a theoretical standpoint (refs, Oberg+11, Ali-Dib+14, Madhusudan+14, Molliere+15, etc.), and volatile snowlines have been detected in disks, such as H₂O and CO (refs). However, both observations and chemical models (refs) have shown that other volatiles are abundant in disks, for example nitrogen bearing species and hydrocarbons, thus shaping the disk composition.
3. Moreover, the snowline locations of these volatiles strongly depend on the grain morphology and the ice environment in which they reside. Laboratory experiments (cite Fayolle+16 and reference therein) have shown that volatiles such as CO and N₂ have significantly different binding energies depending on whether they are pure ices or layered on a water-ice substrate (reference Sections 3 and 4 for details).
4. Thus, there are other important snowlines in disks. Discuss Figure 1. Re-emphasize how this directly changes chemical abundances and C/N/O ratios throughout the disk, and thus the compositions of nascent giant planets.

5. We thus need a more thorough theoretical framework to understand how the processes above affect the C/O and N/O ratios in disks. To address this issue, we expand the coupled drift-desorption model developed in Piso et al. (2015) (hereafter Paper I) by considering additional volatile molecules and abundances, ice morphology, in addition to disk dynamical processes.

2. COUPLED DRIFT-DESORPTION MODEL REVIEW

We begin with a brief review of Paper I's model for the effect of radial drift and viscous gas accretion on volatile snowline locations. We review our disk model in Section 2.1, and summarize our numerical method and results in Section 2.2.

2.1. Disk Model

We first assume a static disk, which is only irradiated by the central star and does not experience redistribution of solids or radial movement of the nebular gas. To quantify the effects of radial drift and gas accretion, we use a viscous disk with a spatially and temporally constant mass flux, \dot{M} . The viscous disk takes into account radial drift, gas accretion onto the central star, as well as accretion heating. We prefer this disk model to an irradiated or evolving disk (see Paper I) because it includes all the dynamical and thermal processes we are interested in for the scope of this paper, and therefore it is the most realistic one.

Following Chiang & Youdin (2010), the temperature profile for a static disk is

$$T = 120 (r/\text{AU})^{-3/7} \text{ K}, \quad (1)$$

where r is the semimajor axis. We use the Shakura & Sunyaev (1973) steady-state disk solution to model the

¹ Harvard-Smithsonian Center for Astrophysics, 60 Garden Street, Cambridge, MA 02138

² Department of Astrophysical Sciences, Princeton University

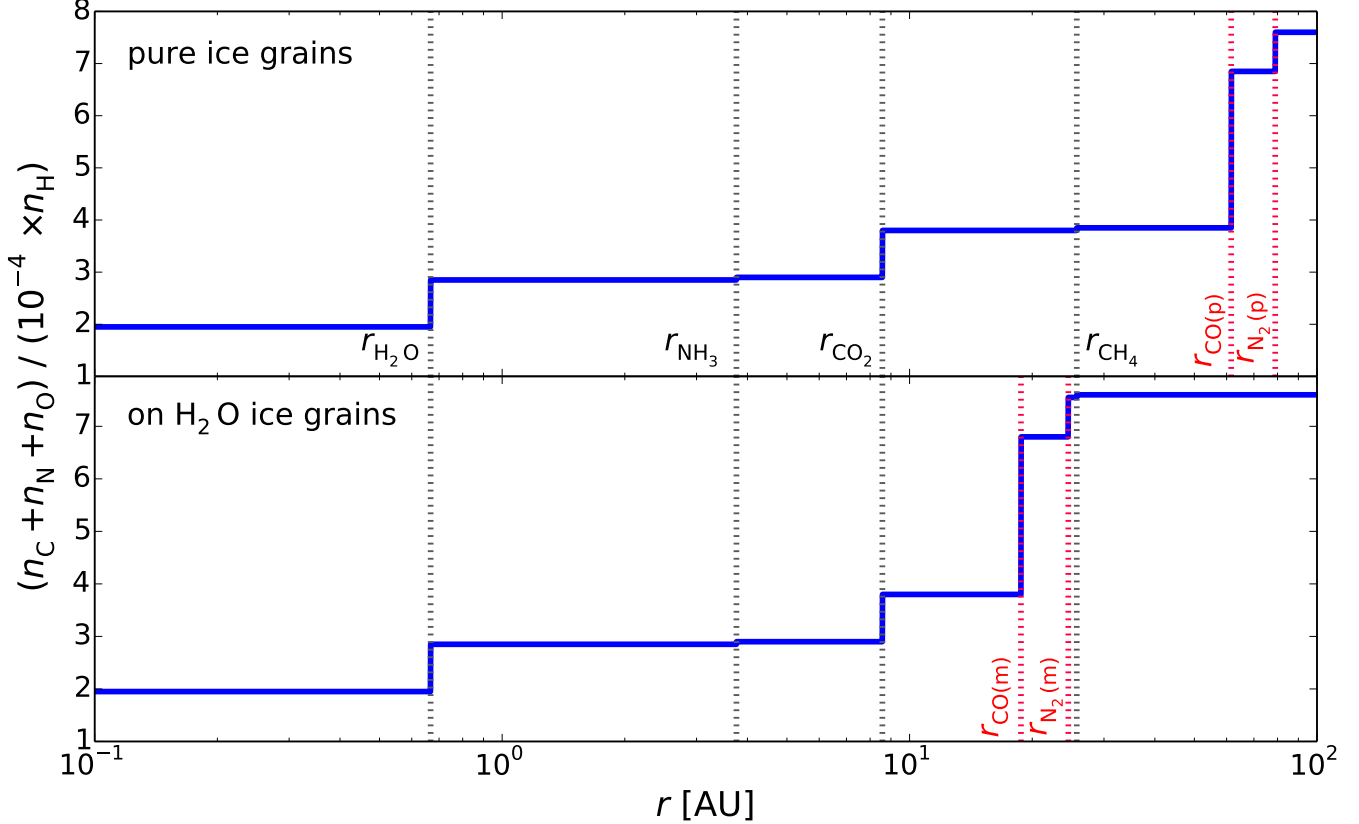


FIG. 1.— The total carbon, nitrogen and oxygen abundance as a function of semimajor axis in a static disk, for CO and N₂ as pure ices (top panel) and layered on a water ice substrate (bottom panel). Relevant volatile snowlines are marked by the vertical dashed lines. The grain abundances are calculated as a function of the observed median CH₄ and NH₃ abundances in protostellar cores (see Sections 3 and 4). The total grain abundance increases with semimajor axis as more and more species freeze out.

viscous disk. From Paper I, the viscous disk temperature profile is computed as

$$T^4 = \left[\frac{1}{4r} \left(\frac{3G\kappa_0 \dot{M}^2 M_* \mu m_p \Omega_k}{\pi^2 \alpha k_B \sigma} \right)^{1/3} \right]^4 + T_{\text{irr}}^4, \quad (2)$$

where $T_{\text{irr}} = T$ from Equation (1). Here G is the gravitational constant, $\kappa_0 = 2 \times 10^{-6}$ is a dimensionless opacity coefficient, $M_* = M_\odot$ is the mass of the central star, $\mu = 2.35$ is the mean molecular weight of the nebular gas, m_p is the proton mass, $\Omega_k = \sqrt{GM_\odot}/r^{3/2}$ is the Keplerian angular velocity, $\alpha = 0.01$ is a dimensionless coefficient (see below for details), k_B is the Boltzmann constant, and σ is the Stefan-Boltzmann constant.

The steady-state disk has an α -viscosity prescription, where the kinematic viscosity is $\nu = \alpha c H$. Here $c \equiv \sqrt{k_B T / (\mu m_p)}$ is the isothermal sound speed (with T from Equation 2), and $H \equiv c / \Omega_k$ is the disk scale height. We can then determine the gas surface density for a viscous disk as (Shakura & Sunyaev 1973; see also Paper I for a more detailed explanation of these calculations):

$$\Sigma = \frac{\dot{M}}{3\pi\nu}. \quad (3)$$

We choose $\dot{M} = 10^{-8} M_\odot \text{ yr}^{-1}$, consistent with mass flux observations in disks (e.g., Andrews et al. 2010). As acknowledged in Paper I, the mass flux rate \dot{M} and stel-

lar luminosity L_* will vary throughout the disk lifetime (Kennedy et al. 2006, Chambers 2009), in contrast with our simplified model which assumes that both quantities are constant. This effect will be most pronounced in the inner disk (\lesssim few AU), where accretion heating dominates. We thus acknowledge that the location of the H₂O snowline may be determined by the decline in \dot{M} or L_* with time, rather than radial drift (see Paper I, Section 2.1 for a more detailed explanation).

2.2. Desorption-Drift Equations and Results

For a range of initial icy grain sizes composed of a single volatile, we showed in Paper I that the timescale on which these particles desorb is comparable to their radial drift time, as well as to the accretion timescale of the nebular gas onto the central star. We thus have to take into account both drift and gas accretion when we calculate the disk location at which a particle desorbs, since that location may be different from the snowline position in a static disk for a given volatile (see Figure 1 and Öberg et al. 2011b). We determine a particle's final location in the disk by solving the following coupled differential equations:

$$\frac{ds}{dt} = - \frac{3\mu_x m_p}{\rho_s} N_x R_{\text{des},x} \quad (4a)$$

$$\frac{dr}{dt} = \dot{r}, \quad (4b)$$

where s is the particle size, t is time, μ_x is the mean molecular weight of volatile x , $\rho_s = 2 \text{ g cm}^{-3}$ is the density of an icy particle, $N_x \approx 10^{15} \text{ sites cm}^{-2}$ is the number of adsorption sites of molecule x per cm^{-2} , $R_{\text{des},x}$ is the desorption rate of species x , and \dot{r} is the particle's radial drift velocity. We calculate R_{des} and \dot{r} as follows.

The desorption rate $R_{\text{des},x}$ (per molecule) is (Hollenbach et al. 2009)

$$R_{\text{des},x} = \nu_x \exp(-E_x/T_{\text{grain}}), \quad (5)$$

where E_x is the adsorption binding energy in units of Kelvin, $T_{\text{grain}} = T$ is the grain temperature (assumed to be the same as the disk temperature, see Paper I), and $\nu_x = 1.6 \times 10^{11} \sqrt{(E_x/\mu_x)} \text{ s}^{-1}$ is the molecule's vibrational frequency in the surface potential well. We discuss our choices for E_x for the different volatile species in Sections 3 and 4.

Following Chiang & Youdin (2010) and Birnstiel et al. (2012), a particle's radial drift velocity can be approximated as

$$\dot{r} \approx -2\eta\Omega_k r \left(\frac{\tau_s}{1 + \tau_s^2} \right) + \frac{\dot{r}_{\text{gas}}}{1 + \tau_s^2}, \quad (6)$$

where the first term is the drift velocity in a non-accreting disk and the second term accounts for the radial movement of the gas. Here $\eta \approx c^2/(2v_k^2)$, where v_k is the Keplerian velocity, and $\tau_s \equiv \Omega_k t_s$ is the dimensionless stopping time:

$$t_s = \begin{cases} \rho_s s / (\rho c), & s < 9\lambda/4 \text{ Epstein drag} \\ 4\rho_s s^2 / (9\rho c \lambda), & s < 9\lambda/4, \text{Re} \lesssim 1 \text{ Stokes drag,} \end{cases} \quad (7)$$

where ρ is the disk mid-plane density, λ is the mean free path and Re is the Reynolds number. The gas accretion velocity \dot{r}_{gas} is determined from $\dot{M} = -2\pi r \dot{r}_{\text{gas}} \Sigma$, for a fixed \dot{M} and with Σ given by Equation (3).

For a particle of initial size s_0 , we solve the Equation set (4) with the initial conditions $s(t_0) = s_0$ and $r(t_0) = r_0$, where t_0 is the time at which we start the integration and r_0 is the particle's initial location. We stop our simulation after $t_d = 3 \text{ Myr}$, the disk lifetime, since this is roughly the timescale on which planets form, and determine the desorption timescale t_{des} from $s(t_{\text{des}}) = 0$, and thus a particle's desorption distance $r_{\text{des}} = r(t_{\text{des}})$. Our results are insensitive to our choice of t_0 as long as $t_0 \ll t_d$. We note that a particle's size is initially fixed and only changes due to desorption. We thus do not take into account processes such as grain coagulation or fragmentation, which nonetheless occur in disks (e.g., Birnstiel et al. 2012, Pérez et al. 2012). We discuss the effect of these processes on snowline locations in Paper I.

As we show in Paper I, a particle of initial size s_0 can experience three outcomes after $t_d = 3 \text{ Myr}$: (1) it can remain at its initial location, (2) it can drift towards the host star, then stop without evaporating significantly, and (3) it can completely desorb on a timescale shorter than 3 Myr. Particles in scenarios (1) and (2) are thus not affected by radial drift or gas accretion, and the snowline locations are those for a static disk. In contrast, the grains in case (3) desorb *instantaneously* and *at a fixed particle-size dependent location* in the disk, regardless of their initial position. The snowline locations for these

particles will thus be fixed for a given initial particle size and disk model. We have found that grains with sizes $\sim 0.001 \text{ cm} \lesssim s \lesssim 7 \text{ m}$ satisfy this condition for our fiducial disk.

3. CH₄ AND C/O RATIOS

Both in Solar system comets and in protoplanetary disks, carbon and oxygen are primarily contained in H₂O, CO₂ and CO (e.g., Rodgers & Charnley 2002, Lodders 2003, Pontoppidan 2006). However, some fraction of the carbon abundance may also be carried by CH₄ (e.g., Mumma et al. 1996), which may change the C/O ratio in gas and in dust throughout the disk. To quantify the magnitude of this effect, we use measured CH₄ abundances in protostellar cores from the *Spitzer* c2d Legacy ice survey (Evans et al. 2003). We explore the parameter space of possible CH₄ abundances by assuming three different scenarios: (1) no CH₄, (2) the median CH₄ observed abundance (hereafter CH₄-mid), and (3) the maximum CH₄ observed abundance (hereafter CH₄-max). Thus $n_{\text{CH}_4\text{-mid}} = 0.0555 \times n_{\text{H}_2\text{O}}$ (Öberg et al. 2011a) and $n_{\text{CH}_4\text{-max}} = 0.13 \times n_{\text{H}_2\text{O}}$ (Öberg et al. 2008), where $n_{\text{H}_2\text{O}}$ is the total H₂O abundance. Similarly to Paper I, we use the H₂O, CO₂ and CO abundances of Öberg et al. (2011b). Since the abundance of carbon grains is uncertain, we assume that all the carbon that is not in the form of CH₄ is found in carbon grains, so that we reproduce the Solar C/O ratio (gas+dust) of 0.54.

We determine the location of the H₂O, CO₂, CO and CH₄ snowlines in our static disk by balancing desorption with readsorption, following Hollenbach et al. (2009). The binding energies of H₂O, CO₂, CO and CH₄ as pure ices are 5800 K, 2000 K, 834 K and 1300 K, respectively (Fraser et al. 2001, Collings et al. 2004, Fayolle et al. 2016, Garrod & Herbst 2006).

Figure 2 shows the C/O ratio in gas and dust as a function of semimajor axis in a static disk, for different CH₄ abundances as outlined above. As in Öberg et al. (2011b) and Paper I, a gaseous C/O ratio of unity can be achieved beyond the CO₂ snowline, where oxygen gas is significantly depleted (top panel). The gas-phase C/O ratio may be further enhanced between the CO₂ and CH₄ snowlines due to the presence of additional carbon gas from CH₄. In this region, the C/O ratio increases by 3% for CH₄-mid and by 8% for CH₄-max, as displayed in the middle and bottom panel of Figure 2. Based on current observations of CH₄ abundances, its presence in the disk only modestly affects the C/O ratio. Given the larger uncertainties in overall volatile abundances, we can neglect CH₄ when estimating the C/O ratio in static disks.

As noted in Section 1, the CO binding energy varies significantly depending on the environment in which the icy grains reside. If CO ice is layered on a water ice substrate, its binding energy will be larger than in the pure ice case (834 K) due to the higher H₂O binding energy. Fayolle et al. (2016) find a CO binding energy of 1388 K in the layered ice scenario. We use the model of Section 2 to estimate the movement of the CO snowline for different grain morphologies in a viscous disk.

Figure 3 shows the H₂O, CO₂ and CO snowline locations for particles with initial sizes $\sim 0.06 \text{ cm} \lesssim s \lesssim 7 \text{ m}$ as well as estimates for the C/O ratio in gas and dust in a viscous disk, with the CO snowline calculated under

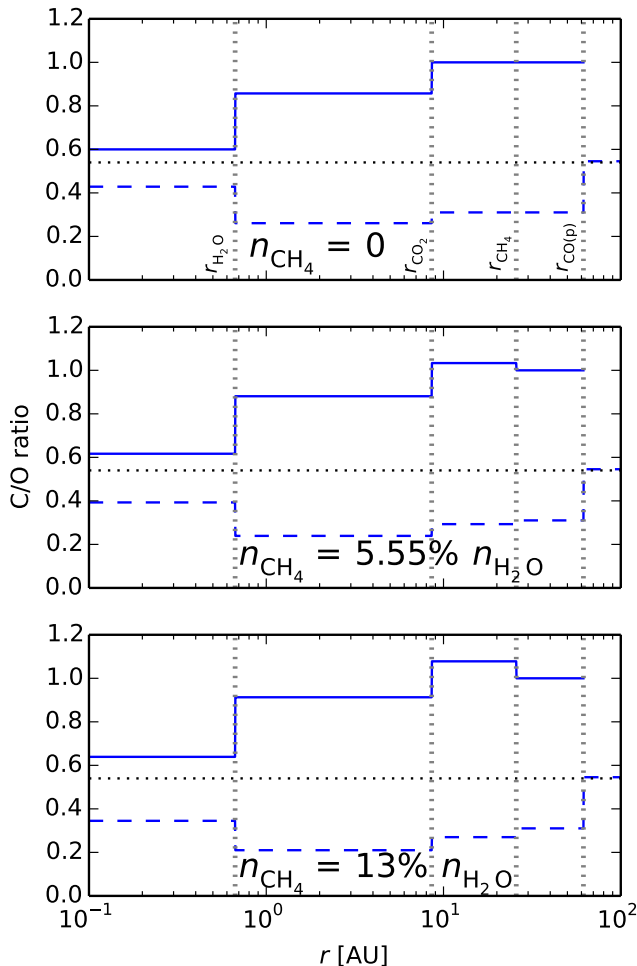


FIG. 2.— The C/O ratio in gas (solid lines) and dust (dashed lines) as a function of semimajor axis in a static disk, assuming no carbon is present in the form of CH_4 (top panel), the median observed CH_4 abundance is assumed (middle panel), and the maximum observed CH_4 abundance is assumed (bottom panel). The C/O estimates are performed assuming that the CO ices are in pure form. The vertical dashed lines mark the snowline locations of the main C and O carriers. The horizontal dashed lines represent the stellar C/O value. The presence of methane only modestly increases the C/O ratio in gas between the CO_2 and CH_4 snowlines.

different grain morphologies as noted above. The true snowline for particles that desorb outside the static snowline is the static snowline itself, hence desorbing particles with $s < 0.06$ cm do not form true snowlines. As calculated in Paper I, drift and gas accretion may move the snowlines inwards by up to 40-60% compared to a static disk, and specifically by up to $\sim 50\%$ in the case of the CO snowline. This result is preserved for the updated CO binding energies, both for pure ice and on a water ice substrate. However, a layered grain structure moves the CO snowline inwards significantly: for our fiducial disk model, $r_{\text{CO,layered}} \approx 8.7$ AU. Thus if CO is bound to water ice instead of pure ices, the CO snowline may move inward by up to 70%. This large inward movement of the CO snowline implies that C/O ratios of order unity may be reached much closer to the host star if CO is layered on a water ice substrate, and the CO snowline may be inside 10 AU for certain disk parameters.

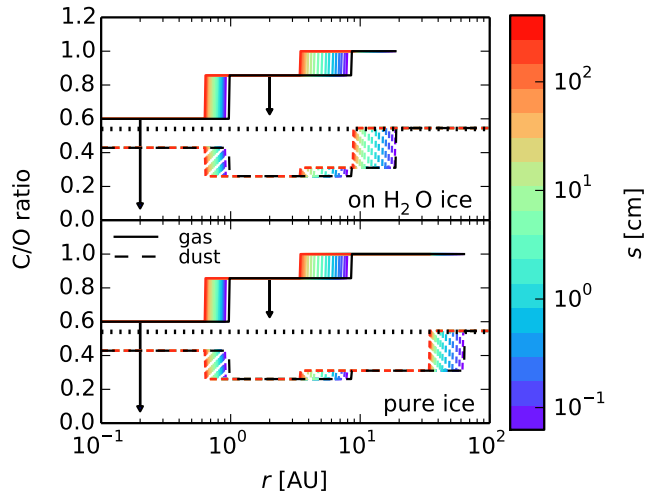


FIG. 3.— C/O ratio estimates in gas (solid lines) and dust (dashed lines) as function of semimajor axis in a viscous disk, for CO residing in a water ice environment (top panel) or as pure CO ice (bottom panel). The H_2O , CO_2 and CO snowlines are shown for particles with initial sizes ~ 0.001 cm $\lesssim s \lesssim 7$ m as indicated by the color bar. The C/O ratio in a static disk (black lines) is shown for comparison. The arrows show that the C/O ratio in gas will decrease inside the H_2O and CO_2 snowlines in the viscous disk, as the relative fluxes of the desorbed icy particles and the overall nebular gas will cause an excess of oxygen gas inside these snowlines (see Paper I for details). Radial drift and gas accretion move the snowlines inward by 40-60%. The presence of CO in a water ice environment rather than as pure ice moves the CO snowline significantly inward by $\sim 70\%$.

4. NITROGEN AND N/O RATIOS

In addition to carbon and oxygen, nitrogen is another abundant volatile in the Solar system and in disks. Chemical models of the protostellar nebula (e.g., Owen et al. 2001) and of protoplanetary disks (e.g., Rodgers & Charnley 2002) suggest that N_2 was the dominant form of nitrogen, and that giant planets have accreted their nitrogen content primarily as N_2 (Mousis et al. 2014). Observations of Solar system bodies such as Titan and Pluto show that N_2 is prevalent in their atmospheres (Cruikshank et al. 1993, Owen et al. 1993). Moreover, the Rosetta spacecraft has recently made the first direct measurement of the N_2 abundance in comet 67P/Churyumov-Gerasimenko (Rubin et al. 2015). In addition to N_2 , a fraction of the nitrogen abundances may be also carried by NH_3 (Bottinelli et al. 2010, Mumma & Charnley 2011).

Because of the high volatility of N_2 , the gas phase nitrogen-to-oxygen (N/O) ratio in the outer disk may be even more enhanced than the C/O ratio compared to its average value in the disk. Giant planets that form at wide separations should thus have an excess of nitrogen in their atmospheres, which could be used to trace their formation origin. In this study, we quantify this effect in protoplanetary disks. We assume that the main nitrogen-bearing species are N_2 and NH_3 , since other volatiles that contain nitrogen have significantly lower abundances in comparison (e.g., Mumma & Charnley 2011). We use the measured total nitrogen abundance in the Solar system, $n_{\text{N}} = 8 \times 10^{-5} n_{\text{H}}$ (Lodders 2003), where n_{H} is the hydrogen abundance in the disk mid-

plane. Similarly to the case of CH_4 (see Section 3), we explore the parameter space of possible NH_3 abundances using data from the Spitzer c2d Legacy ice survey, as follows: (1) no NH_3 , (2) the median NH_3 observed abundance $n_{\text{NH}_3\text{-mid}} = 0.055 \times n_{\text{H}_2\text{O}}$ (Öberg et al. 2011a), and (3) the maximum observed NH_3 abundance $n_{\text{NH}_3\text{-max}} = 0.1537 \times n_{\text{H}_2\text{O}}$ (Bottinelli et al. 2010). In each case, the N_2 abundance then simply follows as $n_{\text{N}_2} = (n_{\text{N}} - n_{\text{NH}_3})/2$. We determine the locations of the N_2 and NH_3 snowlines by balancing desorption with readsorption (Hollenbach et al. 2009), with N_2 and NH_3 pure ice binding energies of 767 K and 2965 K, respectively (Fayolle et al. 2016, Martín-Doménech et al. 2014).

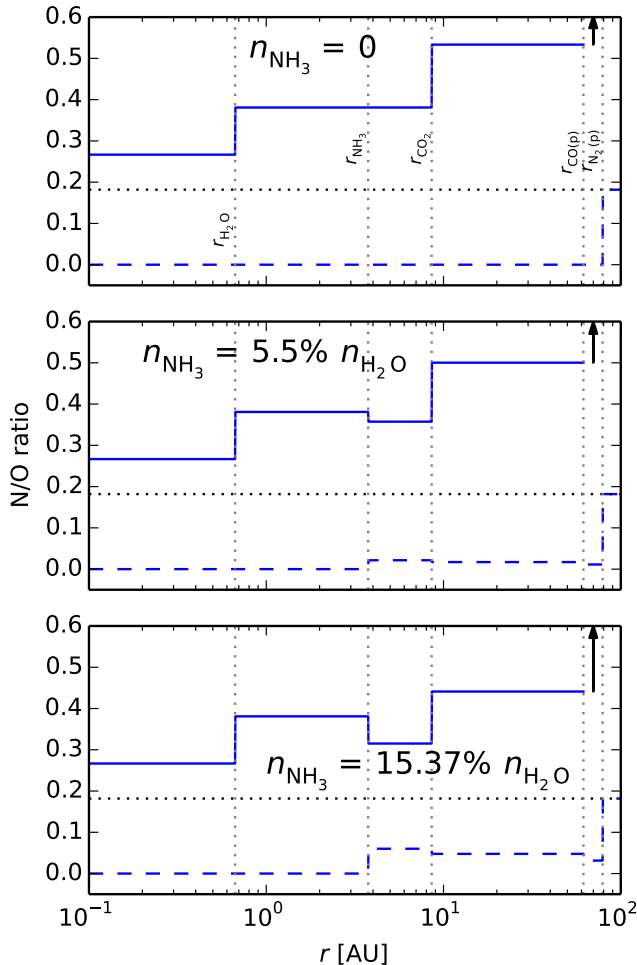


FIG. 4.— The N/O ratio in gas (solid lines) and dust (dashed lines) as a function of semimajor axis in a static disk, assuming no nitrogen is present in the form of NH_3 (top panel), the median observed NH_3 abundance is assumed (middle panel), and the maximum observed NH_3 abundance is assumed (bottom panel). The N/O estimates are performed assuming that the CO and N_2 ices are in pure form. The vertical dashed lines mark the snowline locations of the main C, O and N carriers. The horizontal dashed lines represent the average N/O value in the disk. The gas-phase N/O ratio is highly enhanced in the outer disk (by more than a factor of three) compared to its average value. The arrows mark a highly elevated N/O ratio in gas between the CO and N_2 snowlines due to the depletion of oxygen gas in this region. The presence of NH_3 moderately decreases the N/O ratio in gas between the NH_3 and CO_2 snowlines.

Figure 4 shows the snowline locations of the main oxygen and nitrogen carriers and the N/O ratio in gas and dust as a function of semimajor axis in a static disk, for our three choices of the NH_3 abundance. For comparison, the horizontal dashed line shows the average N/O ratio in the disk. As expected, the gaseous N/O ratio generally exhibits an increasing trend towards the outer disk as more oxygen gas is depleted, with small decreases between the NH_3 and CO_2 snowlines (by 16% for $\text{NH}_3\text{-mid}$ and by 18% for $\text{NH}_3\text{-max}$, respectively) due to NH_3 freeze-out. More importantly, the gas-phase N/O ratio in the outer disk is enhanced by more than a factor of three compared to its average value. This enhancement is more pronounced than the C/O gas-phase enhancement of a factor of two in the outer disk (see Figure 2). The N/O ratio reaches particularly high values between the CO and N_2 snowlines, where all the oxygen is now contained in grains.

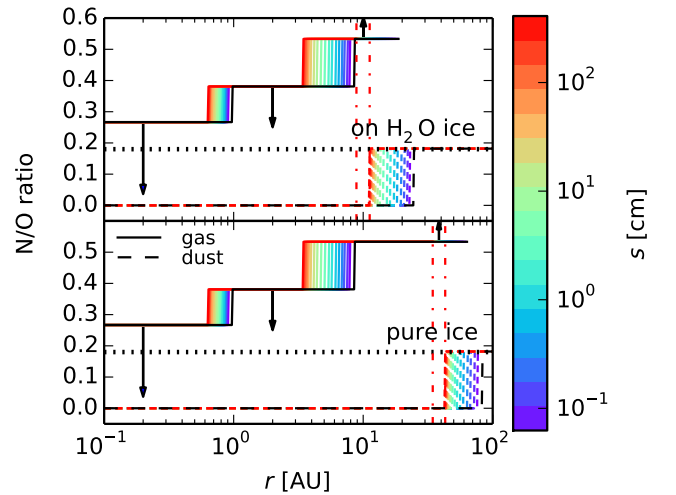


FIG. 5.— N/O ratio estimates in gas (solid lines) and dust (dashed lines) as function of semimajor axis in a viscous disk, for CO and N_2 residing in a water ice environment (top panel) or as pure ices (bottom panel). The H_2O , CO_2 , CO and N_2 snowlines are shown for particles with initial sizes $\sim 0.001 \text{ cm} \lesssim s \lesssim 7 \text{ m}$ as indicated by the color bar. The N/O ratio in a static disk (black lines) is shown for comparison. The arrows show that the N/O ratio in gas will decrease inside the H_2O and CO_2 snowlines in the viscous disk, as the relative fluxes of the desorbed icy particles and the overall nebular gas will cause an excess of oxygen gas inside these snowlines (see Paper I for details). Radial drift and gas accretion move the N_2 snowline inward by up to $\sim 50\%$ compared to a static disk. The presence of N_2 in a water ice environment rather than as pure ice moves the N_2 snowline significantly inward by $\sim 70\%$. The results of highly enhanced gas-phase N/O ratios in the outer disk compared to its average value, and of highly elevated N/O ratios in gas between the CO and N_2 snowlines (see Figure 4), are preserved.

As in the case for CO, the N_2 binding energy is also strongly dependent on the ice environment in which the grain resides. If N_2 is layered on a water ice substrate, the N_2 binding energy is 1266 K (Fayolle et al. 2016). Figure 5 shows the H_2O , CO_2 , CO and N_2 snowline locations in a viscous disk for particles with initial size $\sim 0.06 \text{ cm} \lesssim s \lesssim 7 \text{ m}$, and with the CO and N_2 snowlines calculated assuming different grain morphologies as explained above, as well as estimates for the N/O ratio throughout

the disk. For simplicity, we assume that all nitrogen is bound in N_2 . This choice is justified since the presence of some NH_3 only moderately changes the N/O ratio (see Figure 4), and since we are primarily interested in the N_2 snowline locations rather than exact values for the N/O ratio. The innermost N_2 snowlines in the viscous disk, created by particles with $s \sim 7$ m for our fiducial model, are located at $r_{N_2, \text{pure}} \approx 42$ AU for N_2 as pure ice and at $r_{N_2, \text{layered}} \approx 11$ AU for N_2 layered on water ice. Compared to the static snowlines, i.e. $r_{N_2, \text{pure, static}} \approx 79$ AU and $r_{N_2, \text{layered, static}} \approx 25$ AU, drift and gas accretion move the snowlines inward by up to ~ 50 %, similar to the case for CO (see Section 3). By comparing our results in the viscous disk, we find that the N_2 snowline moves inward by more than 70% if N_2 resides in a water ice environment rather than as pure ice. Similarly to the CO case, the N_2 snowline may be close to or inward of 10 AU for certain disk models.

5. SUMMARY

In this paper we explore the role of icy grain morphology and disk dynamics on the snowline locations of major volatile carrier molecules and the C/N/O ratios in protoplanetary disks. We enhance the coupled drift-desorption model developed in Piso et al. (2015) by adding more carbon- and nitrogen-bearing species into our framework and by considering different environments in which the icy grains reside. Our results can be summarized as follows:

1. Due to the high volatility of N_2 , the gaseous N/O ratio in the outer disk is enhanced by more than a factor of three compared to its average value. This enhancement is more pronounced than in the case of the gas-phase C/O ratio, which is increased by a

factor of two compared to the stellar value. Moreover, the N/O ratio in gas is expected to be very large between the CO and N_2 snowlines due to the complete depletion of oxygen gas in this region

2. The presence of some carbon in the form of CH_4 and of some nitrogen in the form of NH_3 only modestly affects our results for the C/O and N/O ratios, respectively. In both cases, large C/O and N/O ratios in the outer disk are preserved.
3. Grain composition sensitively affects the CO and N_2 snowline locations. If CO and N_2 are layered on a water-ice substrate rather than existing as pure ices, their snowlines move inward by up to ~ 70 %. This effect is separate from that of radial drift and viscous gas accretion, which also cause an inward movement of the CO and N_2 snowlines by up to ~ 50 %.

Our results have direct consequences for the composition of nascent giant planets. The considerable inward movement of the CO and N_2 snowlines due to the ice grains residing in a water ice environment rather than as pure ices implies that giant planets with high C/O and/or N/O ratios in their atmospheres may form closer in than previously predicted by theoretical models. Moreover, our model shows that wide separation gas giants may have an excess of nitrogen in their envelopes, which may be used to trace their origins. In future work, we plan to add new levels of complexity to our model in terms of disk chemistry, dynamics, and planetary dynamics, thus forming a solid framework for understanding the origins of gas giants.

REFERENCES

- Andrews, S. M., Wilner, D. J., Hughes, A. M., Qi, C., & Dullemond, C. P. 2010, *ApJ*, 723, 1241
- Birnstiel, T., Klahr, H., & Ercolano, B. 2012, *A&A*, 539, A148
- Bottinelli, S., Boogert, A. C. A., Bouwman, J., et al. 2010, *ApJ*, 718, 1100
- Chambers, J. E. 2009, *ApJ*, 705, 1206
- Chiang, E., & Youdin, A. N. 2010, *Annual Review of Earth and Planetary Sciences*, 38, 493
- Collings, M. P., Anderson, M. A., Chen, R., et al. 2004, *MNRAS*, 354, 1133
- Cruikshank, D. P., Roush, T. L., Owen, T. C., et al. 1993, *Science*, 261, 742
- Evans, II, N. J., Allen, L. E., Blake, G. A., et al. 2003, *PASP*, 115, 965
- Fayolle, E. C., Balfe, J., Loomis, R., et al. 2016, *ApJ*, 816, L28
- Fraser, H. J., Collings, M. P., McCoustra, M. R. S., & Williams, D. A. 2001, *MNRAS*, 327, 1165
- Garrod, R. T., & Herbst, E. 2006, *A&A*, 457, 927
- Hollenbach, D., Kaufman, M. J., Bergin, E. A., & Melnick, G. J. 2009, *ApJ*, 690, 1497
- Kennedy, G. M., Kenyon, S. J., & Bromley, B. C. 2006, *ApJ*, 650, L139
- Lodders, K. 2003, *ApJ*, 591, 1220
- Martín-Doménech, R., Muñoz Caro, G. M., Bueno, J., & Goesmann, F. 2014, *A&A*, 564, A8
- Mousis, O., Fletcher, L. N., LEBRETON, J.-P., et al. 2014, *Planet. Space Sci.*, 104, 29
- Mumma, M. J., & Charnley, S. B. 2011, *ARA&A*, 49, 471
- Mumma, M. J., Disanti, M. A., dello Russo, N., et al. 1996, *Science*, 272, 1310
- Öberg, K. I., Boogert, A. C. A., Pontoppidan, K. M., et al. 2008, *ApJ*, 678, 1032
- . 2011a, *ApJ*, 740, 109
- Öberg, K. I., Murray-Clay, R., & Bergin, E. A. 2011b, *ApJ*, 743, L16
- Owen, T., Mahaffy, P. R., Niemann, H. B., Atreya, S., & Wong, M. 2001, *ApJ*, 553, L77
- Owen, T. C., Roush, T. L., Cruikshank, D. P., et al. 1993, *Science*, 261, 745
- Pérez, L. M., Carpenter, J. M., Chandler, C. J., et al. 2012, *ApJ*, 760, L17
- Piso, A.-M. A., Öberg, K. I., Birnstiel, T., & Murray-Clay, R. A. 2015, *ApJ*, 815, 109
- Pontoppidan, K. M. 2006, *A&A*, 453, L47
- Rodgers, S. D., & Charnley, S. B. 2002, *MNRAS*, 330, 660
- Rubin, M., Altwegg, K., Balsiger, H., et al. 2015, *Science*, 348, 232
- Shakura, N. I., & Sunyaev, R. A. 1973, *A&A*, 24, 337